Title

Optimizing LA-ICP-MS analytical procedures for elemental depth profiling of foraminifera shells

Authors

Fehrenbacher, Jennifer S
Spero, Howard J
Russell, Ann D
et al.

Publication Date

2015-06-01

DOI

10.1016/j.chemgeo.2015.04.007

Peer reviewed

Chemical Geology 407–408 (2015) 2–9

Contents lists available at ScienceDirect

Chemical Geology

journal homepage: www.elsevier.com/locate/chemgeo

Optimizing LA-ICP-MS analytical procedures for elemental depth profiling of foraminifera shells

Jennifer S. Fehrenbacher [a,*], Howard J. Spero [a,1], Ann D. Russell [a,2], Lael Vetter [b], Stephen Eggins [c,3]

[a] Department of Earth and Planetary Sciences, University of California, Davis, One Shields Avenue, Davis, CA 95616-8605, USA
[b] Department of Earth and Environmental Sciences, Tulane University, 6823 St. Charles Avenue, New Orleans, LA 70118, USA
[c] Research School of Earth Sciences, The Australian National University, Canberra 0200, Australia

ARTICLE INFO

Article history:
Received 17 December 2013
Received in revised form 10 April 2015
Accepted 11 April 2015
Available online 27 April 2015

Editor: Michael E. Böttcher

Keywords:
Laser ablation ICP-MS
Foraminifera
Depth profiling
Trace metals

ABSTRACT

Laser ablation inductively coupled plasma mass spectrometry (LA-ICP-MS) is becoming a widespread technique for analyzing elemental ratios in foraminiferal calcite. Here we focus on optimizing LA-ICP-MS for high-resolution depth profiling of elemental ratios through shell walls. This application reveals intrashell variability and provides a unique opportunity to quantify trace element incorporation over short time scales of calcification by an individual foraminifer. High-resolution depth profiling requires careful consideration of both ablation and analytical conditions required to resolve differences in shell chemistry across sub-micron shell thickness. We present laser ablation profiles of NIST SRM 610 standard glass data (in cps) and elemental/Ca ratios (in mmol/mol) from foraminiferal calcite obtained over a range of operating conditions using a Photon Machines 193 nm UV excimer laser-ablation system, equipped with a dual-volume ANU HelEx chamber, coupled to an Agilent 7700x quadrupole ICP-MS. Different combinations of energy density, repetition rate, and mass spectrometer cycle time can yield varying elemental profiles. This variability can mimic and/or mask real intrashell trace element heterogeneity in foraminifer shells. At low (<3 Hz) laser repetition rates, real intrashell element variation can be obscured depending on the laser energy, whereas using moderate (≥3 Hz) laser repetition rates and/or a signal-smoothing device improves the accuracy and precision of intrashell trace element profiles. Shell material is ablated rapidly when using a 5 Hz or greater repetition rate and an energy density of 3 J/cm^2 or greater, resulting in reduced spatial resolution.

1. Introduction

Analyses of the elemental composition of foraminifera shells is a fundamental component of paleoceanographic studies of past ocean temperature and chemistry. Paleoenvironmental reconstructions of seawater temperature (Mg/Ca) (Lea et al., 1999; Nurnberg et al., 1996), pH and carbonate chemistry (U/Ca, Mg/Ca, B/Ca, Zn/Ca, Li/Ca) (Allen et al., 2012; Marchitto et al., 2005; Russell et al., 2004; Yu and Elderfield, 2007), and nutrients (Cd/Ca, Ba/Ca, Zn/Ca) (Boyle, 1988) rely on measurements of trace element/Ca (TE/Ca) ratios in fossil foraminifera (for a thorough review see (Katz et al., 2010) and references therein). TE/Ca ratios have traditionally been measured on multiple shells in solution via inductively coupled plasma (ICP) mass spectrometry (-MS) or atomic emission spectrometry (-AES) (Anand et al., 2003; Barker and Elderfield, 2002; de Garidel-Thoron et al., 2007; de Villiers, 2003; Fehrenbacher et al., 2006; Lea et al., 2000; Lea et al., 1999; Martin et al., 2002; McConnell and Thunell, 2005; Nurnberg and Groeneveld, 2006; Regenberg et al., 2006; Rosenthal and Lohmann, 2002; Rosenthal et al., 1999; Russell et al., 2004; von Langen et al., 2005). TE/Ca ratios yield average environmental conditions experienced by the population of shells analyzed. However, additional ecologic, physiologic, environmental, and/or diagenetic information is recorded in the TE/Ca ratios of individual shells and intrashell TE/Ca patterns (particularly Mg/Ca), which can be measured in individual foraminifera using high-resolution techniques, such as laser ablation (LA-) ICP-MS or electron microprobe analysis (EMPA) (e.g. Eggins et al., 2003; Eggins et al., 2004; Sadekov et al., 2009; Fehrenbacher and Martin, 2010).

Wu and Hillaire-Marcel (1995) were the first researchers to use LA-ICP-MS to analyze the trace element composition of foraminifera (Wu and Hillaire-Marcel, 1995), and over the last decade quantification of average and intrashell TE/Ca variability using LA-ICP-MS has expanded rapidly (e.g. Bolton et al., 2011; Creech et al., 2010; Duenas-Bohorquez et al., 2009; Eggins et al., 2003; Hathorne et al., 2009; Hathorne et al., 2003; Raitzsch et al., 2010; Raitzsch et al., 2011; Sadekov et al., 2009; Sadekov et al., 2010; Wit et al., 2010; Wit et al., 2012). For example, recent studies explored Mg/Ca ratios in single foraminifera shells and individual chambers to develop temperature calibrations (Marr et al.,

* Corresponding author. Tel.: +1 530 752 9225.
E-mail addresses: jfehrenbacher@ucdavis.edu (J.S. Fehrenbacher), hjspero@ucdavis.edu (H.J. Spero), adrussell@ucdavis.edu (A.D. Russell), lvetter@ucdavis.edu (L. Vetter), Stephen.Eggins@anu.edu.au (S. Eggins).
[1] Tel.: +1 530 752-3307.
[2] Tel.: +1 530 752-3311.
[3] Tel.: +61 2 612 59965.

http://dx.doi.org/10.1016/j.chemgeo.2015.04.007
0009-2541/

2011; Sadekov et al., 2009), compared to single-chamber Mg/Ca ratios with whole shell $\delta^{18}O$ analyses (Wit et al., 2010), detailed how to examine and identify pristine portions of calcite in diagenetically altered shells (Creech et al., 2010), and examined mechanisms of foraminifera biomineralization using living foraminifers grown in controlled laboratory experiments (Spero et al., 2015; Vetter et al., 2013a). The potential for future paleoceanographic applications is only beginning to be fully appreciated.

Generating high-resolution depth profiles of intrashell TE/Ca variability in foraminifera shells that display variation on <1 μm spatial scales requires using 1) low laser energy density, 2) low laser repetition rates, and 3) a deep UV laser (ideally 193 nm (Eggins et al., 2003, 2004), although 213 nm has also been shown to couple reasonably well with calcite (Hathorne et al., 2009; Jeffries et al., 1998)). Under these conditions the laser removes a thin layer of calcite during each laser pulse (< a few hundred nm), thereby allowing the user to produce data with sub-micron spatial resolution. However, user-defined parameters such as laser repetition rate and mass spectrometer cycling time (dependent on the isotopes of interest) can have a significant effect on the quality of TE/Ca data. Interference between repetition rate and cycling time can result in harmonic interference patterns (referred to as spectral skew) (Müller et al., 2009; Pettke et al., 2000). These interferences can obscure real intrashell TE/Ca patterns and render intrashell variations difficult or impossible to evaluate. Interpretation is particularly problematic when the data are normalized using an internal standard, because the timing of the interference patterns is shifted for each isotope (Fig. 1).

In this study, we present data that illustrate how the LA-ICP-MS operational parameters influence the quality and spatial resolution of the data produced. We present data from a NIST SRM 610 glass standard using different mass spectrometer cycle times and repetition rates, both with and without a 10-path distributed delay manifold (a 'squid') (Eggins et al., 1998a), to illustrate how different repetition rates, cycle times, and the use of a squid affect the relative standard deviations (RSDs) of the isotopes analyzed. The 'squid' attenuates the effect of using a low laser repetition rate with an ablation cell that has a rapid washout time.

We then document the influence of repetition rate, energy density, and the presence or absence of a squid on the precision and reproducibility of intrashell Mg/Ca depth profiles through foraminiferal calcite by generating repeat ablation profiles on a single *Orbulina universa* shell. *O. universa* is an ideal species to use because the shell is composed of a single spherical chamber that displays significant intrashell Mg/Ca variation (Mg/Ca 'banding') that is evenly distributed around the entire test (Figure S1) (cf. Eggins et al., 2003). Specimens of *O. universa* can be broken into multiple fragments that permit the user to repeat depth profile analyses on a single *O. universa* shell and many profiles can be generated on the same shell without distortion due to curvature of the shell wall. We present data from numerous analytical sessions in our laboratory that demonstrate the reproducibility of this intrashell variability, thereby permitting us to directly compare ablation results from multiple depth profiles obtained using different instrument conditions across different analytical sessions. While we focus here on optimizing depth profiles through shell walls of foraminifera, our approach can be adapted for high-resolution depth profiling through any material.

2. LA-ICP-MS methods, experimental procedures, and samples

2.1. Methods

Trace element profiles were obtained using a Photon Machines 193 nm ArF UV excimer laser with an ANU HelEx dual-volume laser ablation cell coupled to an Agilent 7700x quadrupole-ICP-MS (non-varying parameters are summarized in Table 1; experimental parameters are detailed in Table 2). Ablated material flows to the ICP-MS in a He gas mixture. When the squid is installed, we inject Ar into the He stream between the ablation cell and the squid to improve transmission of ablated material. Gas composition and flow rate are determined by adjusting the flow of Ar and He as necessary to achieve high count rates on the sample/standard while maintaining ThO^+/Th^+ oxide ratios

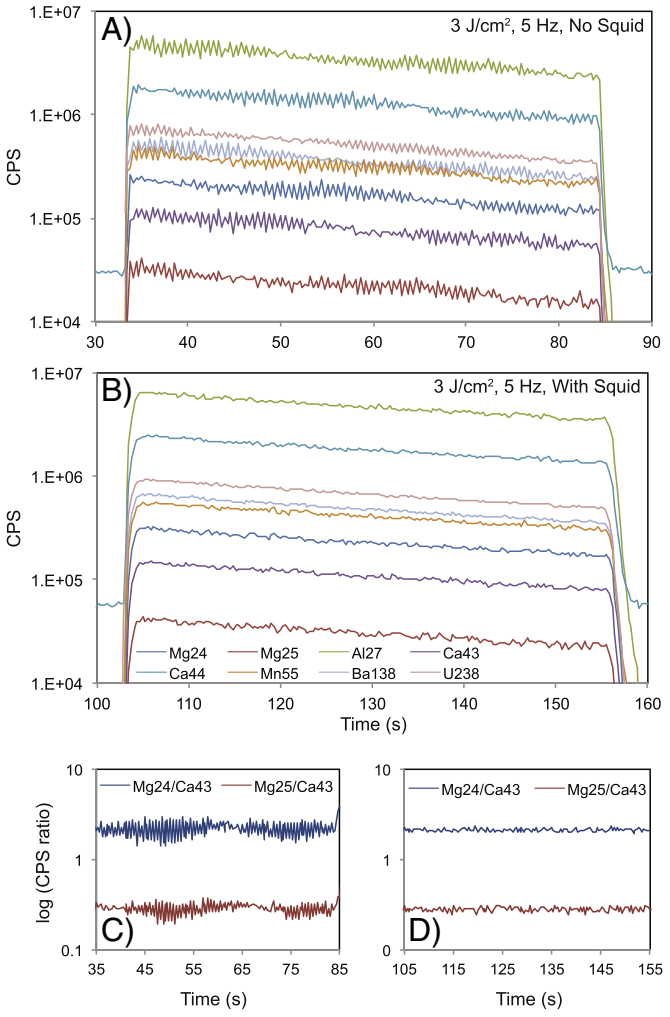

Fig. 1. Ablation profiles generated on a NIST SRM610 glass standard using laser energy density set at 3 J/cm², a repetition rate of 5 Hz, and a 40-μm spot size. (A) Profile generated without a squid installed. Note difference in the timing of the harmonic-like patterns in the different isotopes caused by spectral skew. This offset in timing produces large oscillations in the TE/Ca ratios when using a ^{43}Ca internal standard. (B) Profile generated with a squid installed. Note the absence of spectral skew in this profile. The smoothed data do not yield oscillations in the ratios when using an internal standard. (C) The ratios of $^{24}Mg/^{43}Ca$ and $^{25}Mg/^{43}Ca$ generated using the data in Fig. 1A. Note the high-amplitude offset oscillations. (D) The ratios of $^{24}Mg/^{43}Ca$ and $^{25}Mg/^{43}Ca$ generated using the data from Fig. 1B. Note the smoothing effect of the squid.

Table 1
Summary of operating conditions of the laser ablation and ICP-MS; only those that remain constant throughout all the experiments are presented here.

ICPMS: Agilent 7700x	
RF power	1500 W
Argon (carrier) gas flow	0.95–1.05 l/min (tuned daily)
Ar coolant gas flow	15 l/min
Ar auxiliary gas flow	1 l/min
Dwell time per mass	20–100 ms (variable)
Laser-ablation system: UV excimer laser	
Energy density (fluence)	1–4.5 J/cm² (variable)
He gas flow	1.05 l/min
Laser repetition rate	1–8 Hz
Laser spot size	40 μm
ThO^+/Th^+	<0.5%
U^+/Th^+	~1

Table 2
Isotope menus, dwell times, and total sweep times for each analytical method used.

Method	Method description	Isotope menu	Dwell time (ms)	Total sweep time (ms)*	Material
1	Constant dwell time	^{24}Mg, ^{25}Mg, ^{27}Al, ^{43}Ca, ^{44}Ca, ^{55}Mn, ^{88}Sr, ^{138}Ba	10	96	NIST SRM610
2	Foram analogue, variable dwell time	^{24}Mg, ^{25}Mg, ^{27}Al, ^{43}Ca, ^{44}Ca, ^{55}Mn, ^{88}Sr, ^{138}Ba	Variable (10–50 ms)	226	NIST SRM610
3	Foram analogue with low-abundance elements, variable dwell time	^{24}Mg, ^{25}Mg, ^{27}Al, ^{43}Ca, ^{44}Ca, ^{55}Mn, ^{88}Sr, ^{138}Ba, ^{7}Li, ^{66}Zn, ^{111}Cd, ^{238}U	Variable (10–50 ms)	416	NIST SRM610
4	Constant dwell time	^{24}Mg, ^{25}Mg, ^{27}Al, ^{43}Ca, ^{44}Ca, ^{55}Mn, ^{88}Sr, ^{138}Ba	100	816	NIST SRM610
5	Variable dwell time, foram analogue used to generate Figs. 2 and 3	^{24}Mg, ^{25}Mg, ^{27}Al, ^{43}Ca, ^{44}Ca, ^{55}Mn, ^{138}Ba, ^{238}U	Variable (10–50 ms)	309	Foram calcite

*Includes time for peak hopping (average 1.5 ms).

less than 0.5% (tuned daily). For the analyses of the NIST glass, we also tune to produce robust plasma conditions by maintaining U^+/Th^+ ratios near ~1 and ThO^+/Th^+ <0.5% (Eggins et al., 1998b; Gunther and Hattendorf, 2005).

2.2. Glass standard analytical procedure

To explore the interactions between laser repetition rate and mass spectrometer cycle time, both with and without a squid, we analyzed NIST SRM 610 glass using four different isotope menus (Methods 1–4, Table 2). The total acquisition (cycle/sweep) time varied between 96 ms and 816 ms depending on the isotope menu and dwell times (Table 2). We use an energy density of 4.5 J/cm^2 for all glass analyses and vary the repetition rate of the laser between 1 and 8 Hz. Note that low repetition rates incur corresponding lower signal intensities that can compromise the analysis. However, we include low repetition rates here for comparison to data obtained on a different laser ablation system (Resonetics RESOlution M50 system (Müller et al., 2009); See Section 3.1). We collect ~50 s of background intensities and then ablate the glass standard for 90 s at each repetition rate (1–8 Hz). Between each increase in repetition rate, we separate analyses with a 10-second period with the laser off to allow counts to return to background levels. We observe that on our system, a 99% signal washout occurs within ~1.5 s without the squid attached (effectively complete within ~2 s) and a 99% signal washout occurs within 2 s with the squid attached (effectively complete within 3.5 s) (Figure S2). The complete washout time using the ANU HelEx cell with the squid attached is faster than that reported by Müller et al., 2009 using a Resonetics RESOlution M50 system (cf. 99% signal washout within 3.5 s, complete washout in 9 s) (Müller et al., 2009).

2.3. Foraminifer analytical procedure

2.3.1. Foraminifer specimen selection and cleaning

For the foraminifer analyses we use a single *O. universa* shell obtained from the >500 μm size fraction of the 18–20 cm interval in core MW91-9 6GGC (2°12.54′S, 156°57.9′E, 1.6 km water depth, Ontong Java Plateau, western equatorial Pacific). This interval corresponds to the early Holocene (~8.5 ka) (Fehrenbacher and Martin, 2011). The spherical chamber of *O. universa* contains measurable quantities of all the cations currently used for paleoceanographic analyses (e.g. B, Mg, Ca, Ba, Sr, Zn). We also show depth profiles from a cultured *Neogloboquadrina dutertrei* shell that was previously analyzed via electron microprobe image mapping (Fehrenbacher et al., 2011) (see Fehrenbacher and Martin, 2010 for EMPA methodology). EMPA results on one (F-1) and two (F-2) chambers before the final (F) chamber show this shell has lower intrashell Mg variation in comparison to *O. universa*. Mg/Ca banding is present but of lower amplitude compared to *O. universa*. Here, we analyze the final chamber from the remaining portion of the shell using the optimized laser ablation settings determined in this study (Section 3.2.2).

The foraminifer shells were cleaned prior to analysis. For *O. universa,* the shell was gently split open after placing it in a drop of water on a large rubber stopper and cracking the shell with a scalpel. The rubber stopper provides an elastic surface that gives under the pressure of the scalpel and the water helps keep the shell from shattering (Shuxi and Shackleton, 1990), thereby yielding the largest recoverable fragments. The fossil *O. universa* fragments were subsequently cleaned to remove finely adhering clays by repeat rinses (3×) in ultra-pure water (>18 MΩ), followed by a methanol rinse that included a brief ultrasonication (2–5 s) and a final ultra-pure water rinse. Cleaned fragments were inspected under a microscope and fragments that appeared dirty were rinsed again. We did not subject the fossil foraminifer to the full cleaning method that includes oxidative and reductive cleaning steps because initial analyses indicated the foraminifers subjected to the rinse step only did not contain high levels of manganese, aluminum, or barium, which would have indicated further cleaning steps were necessary (Vetter et al., 2013b). The cultured *N. dutertrei* shell was subjected to an oxidative cleaning in a buffered hydrogen peroxide solution (1:1 mixture of 30% H_2O_2 and 0.1 N NaOH) for 30 min at 65 °C to remove remnant organic matter, followed by 3 rinses in ultra-pure water (>18 MΩ). *O. universa* shell fragments were placed on double-sided carbon tape on glass slides, with the inside of the shell facing up, to enable high resolution profiling of *O. universa* (Eggins et al., 2003; Eggins et al., 2004). In contrast, the fragment of the *N. dutertrei* shell was ablated with the inside of the shell facing down to analyze the most recent calcite that was added to the outside of the shell in culture.

2.3.2. Foraminifer laser ablation methods

We analyzed the foraminifers using mass spectrometer Method 5 (Table 2) and only report Mg/Ca ratios. In many samples, the U concentration was below our detection limit (5 ppb) and shell Ba content is invariant through the shell of this species (Vetter et al., 2013b). The Mg/Ca ratios for the foraminifera were calculated offline in MS Excel, following data reduction protocols detailed in Longerich et al. (1996), that include screening for outliers, drift correcting by bracketing samples with NIST SRM 610 analyses, and subtracting background count rates from each data point. Mg/Ca ratios were calculated by normalization to the known trace element concentrations in the drift-corrected bracketed analyses of the NIST SRM 610 standard (Mg = 432 μg/g, Ca = 81,830 μg/g (Jochum et al., 2011)). We use ^{43}Ca as our internal standard. ^{44}Ca is monitored to check for consistency and ^{27}Al and ^{55}Mn are monitored to identify surface contamination and as an indicator of shell profile analysis completion and subsequent ablation of the carbon tape (which yields a diagnostic signal at ^{27}Al). We obtain the integrated average Mg/Ca ratio after excluding an initial elemental spike that could be surface contamination or excess ablated material from the shell surface (see Figure S3). A single randomly selected *O. universa* shell (>600 μm diameter), cleaned as described above, is analyzed 1–5 times during each analytical session to assess reproducibility during and between analytical sessions. This shell is used as a consistency standard

for depth profiling (Section 3.3) and is not the same specimen used to generate Figs. 3 and 4 below.

3. Results and discussion

3.1. NIST SRM 610 analyses

Laser ablation line analyses (lateral tracks on the surface of the glass) are detailed in Figures S4–S8. The relative standard deviations for all methods with and without the squid are detailed in Fig. 2 (data reported in Table S1).

3.1.1. Analyses without a squid

The relative standard deviations (RSDs, an indicator of the noisiness of the signal) are high at 1 Hz laser repetition rate, decrease between 2–4 Hz, and begin to stabilize when the repetition rate exceeds 4 Hz, (Fig. 2, blue symbols, Figure S4, Table S1). Using a repetition rate of 1 Hz, the signal is highly variable regardless of mass spectrometer cycle time (Figure S4). RSDs are highest (Table S1, 47–60%) when the mass spectrometer dwell time per element is short (10 ms, Method 1, Fig. 2A, cycle time 96 ms) and decrease to 1–2% as the dwell times approach 100 ms and the counting statistics improve, thereby leaving only the component of noise related to signal variability. The MS cycle times in Methods 2 and 3 (226 ms to 416 ms, Fig. 2B and C) represent MS cycle times typical of foraminifer analyses in other studies. Method 3 includes isotopes that require longer dwell times owing to their low abundances in foraminifers (50 ms for each isotope). The RSDs using Method 2 level off to ~4–5% when the laser repetition rate is ≥4 Hz (Fig. 2B, blue symbols). Using the longer MS cycle time in Method 3, the RSDs do not level off until the laser repetition rate is ≥5 Hz (Fig. 2C, blue symbols). The smoothest signal is achieved when the dwell time is longest (100 ms, Method 4, total cycle time 816 ms, Fig. 2D). However, this MS cycle time is too long to fully resolve transitions in intrashell foraminiferal Mg/Ca because these transitions occur over short spatial scales. Figures S5–S8 (expanded portions of Figure S4) highlight the variable nature of the pulsed signal at lower repetition rates (2 and 3 Hz) and the improvement in the signal at higher repetition rates (5 Hz). These figures also illustrate how the signal can vary depending on the isotope of interest (compare Figures S5 and S6 to Figures S7 and S8).

3.1.2. Analyses with a squid

A visual comparison of data with and without the squid demonstrates the reduced RSDs obtained when the squid is installed (Fig. 2, black vs. blue symbols). Nevertheless, the RSDs still exceed 15% at 1 Hz (Figure S4, Table S1). This result contrasts with data by Müller et al. (2009) who demonstrated a smooth signal at repetition rates as low as 1 Hz. These differences could be linked to the slower washout times of their squid and/or longer residence time of their ablation cell design. In the Photon Machines system, the signal RSDs decrease rapidly between 2 and 3 Hz when the squid is installed, depending on the cycle time, the isotope of interest, and ICP-MS sensitivity (e.g., ^{25}Mg, ^{66}Zn, ^{111}Cd have higher RSDs). Similar to the results obtained without the squid, the RSDs are highest when the dwell times are short (10 ms) and lowest as the dwell times approach 100 ms. RSDs range from 2 to 4% when the dwell times are similar to those used in foraminifer analyses with little improvement in the RSDs with repetition rates that exceed 4 Hz. The expanded portions of the Mg/Ca (cps/cps) and Sr/Ca

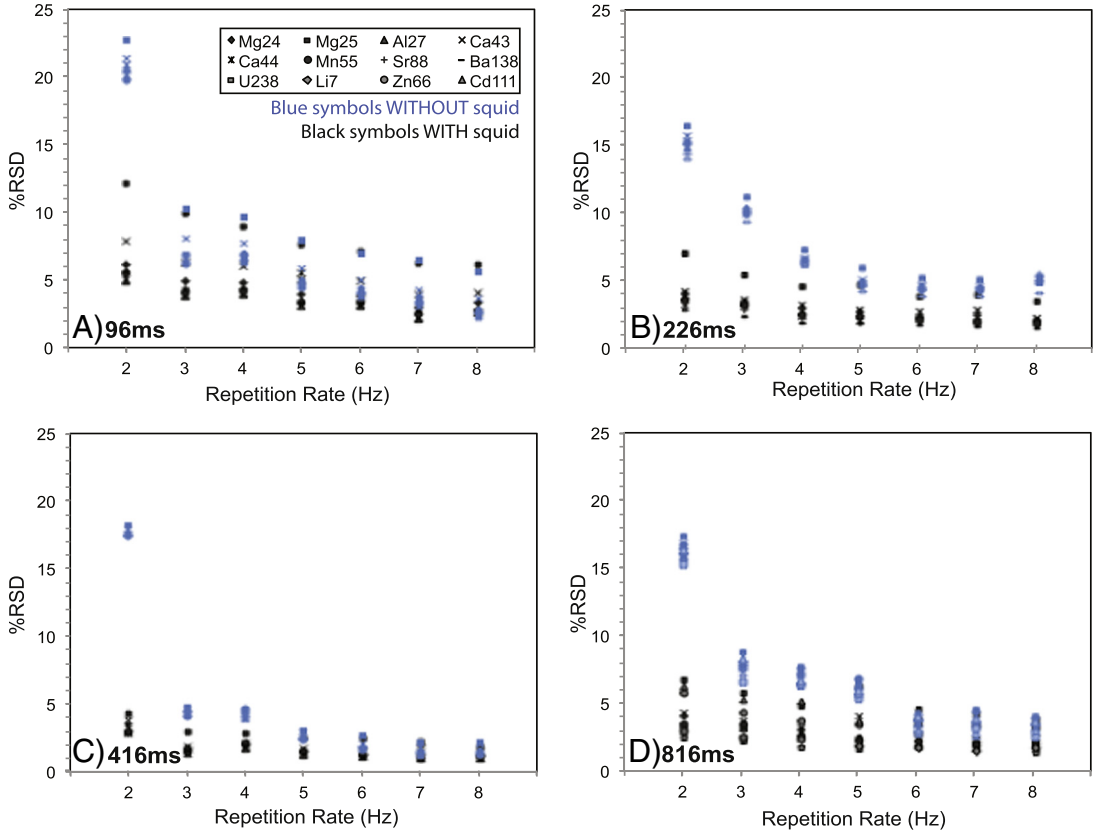

Fig. 2. Relative standard deviations (RSDs) versus repetition rate for the isotope data presented in Figure S1. The RSDs are shown for each isotope at each corresponding repetition rate both with (black symbols) and without (blue symbols) the installation of a squid for the four mass spectrometer cycle methods detailed in Table 1. (A) Method 1: 96 ms cycle time, (B) Method 2: 226 ms cycle time, (C) Method 3: 416 ms cycle time, and (D) 816 ms cycle time. (For interpretation of the references to color in this figure legend, the reader is referred to the web version of this article.)

(cps/cps) from Figure S4 demonstrate the benefit of using a squid (Figures S5–S8). For example, at low repetition rates and short dwell times (10 ms), a smooth signal can be achieved for ^{24}Mg (e.g. 2 or 3 Hz; Figure S5D–E) with only a moderate improvement in the RSD at higher repetition rates (S5F). Increasing the dwell times slightly (to 20 ms) yields an even smoother signal (Figure S5J–L). However, this does not apply to Sr/Ca data where a much more rapid repetition rate and longer dwell time are needed to provide a smooth signal (compare Figures S5 and S6 to Figures S7 and S8).

3.2. O. universa analyses

In Figs. 3 and 4 below, the time resolved analyses were converted to depth (i.e. shell thickness) by calibrating the pit depth vs. laser pulse relationship. We generated 9 laser ablation 'pits' in a fossil *O. universa* using 1, 2, and 3 J/cm^2 each and 200 laser pulses (3 replicate ablation pits at each energy). Pit depths were then measured on an SEM to calibrate the depth/laser ablation rates to convert laser ablation rate into shell thicknesses.

3.2.1. Depth profiles without a squid

Depth profile data collected from *O. universa* without a squid contain high-amplitude, high-frequency oscillations in the Mg/Ca ratios in nearly all ablation profiles, with the exception of those generated with a 5 Hz repetition rate (the maximum pulse rate tested on foraminifers in this study) (Fig. 3). These oscillations are not due to real intrashell Mg/Ca variability. Rather, they arise from spectral skew due to the interplay between the transient signal produced by the laser (laser repetition rate-induced) and the cycle time of the ICP-MS (~300 ms), which reflects the interference (beat pattern) between the laser pulse and mass spectrometer cycle frequencies. In this experiment, the amplitude of these high-frequency Mg/Ca oscillations, which can exceed 14 mmol/mol, is largest when the energy density is 1 J/cm^2 and the repetition rate is ≤4 Hz (Fig. 3A–C). Natural intrashell Mg/Ca variation in foraminifera has a much longer wavelength and the amplitude is typically lower than the magnitude of these oscillations (Eggins et al., 2004; Spero et al., 2015). Note that the Mg/Ca range encompassed by these high amplitude oscillations can vary among depth profiles generated on the same sample, even using identical settings, because the operator-dependent offset between the start of the mass spectrometer cycle and the start of laser pulsing is different for each ablation depth profile. The amplitude of the oscillations is largest when the repetition rate is 3 Hz, regardless of the energy (Fig. 3B, F, and J). We attribute this to the generation of a beat effect when we use a repetition rate that is nearly the same as the mass spectrometer cycle time. To further illustrate how the repetition rate and cycle time coherence can be problematic, we analyze the same fragment using a repetition rate of 6 Hz. At the higher repetition rate of 6 Hz, oscillations are similar to the repetition rate at 3 Hz because the pulse rate is a multiple of the cycle time (~300 ms) (Figure S9). However, when pulse rate is 5 Hz (Fig. 3L), the high-amplitude oscillations are absent.

A smooth signal that accurately captures intrashell variation is achieved at 5 Hz and 1–2 J/cm^2 energy density. Using this combination, the measured signal intensities are greater, the repetition rate exceeds the cycle time of the mass spectrometer, and the supply of ablated material is more uniform, thereby producing a smoother signal (Fig. 3D and H). At higher energy (3 J/cm^2) the spatial resolution of features within the depth profile decreases, as each

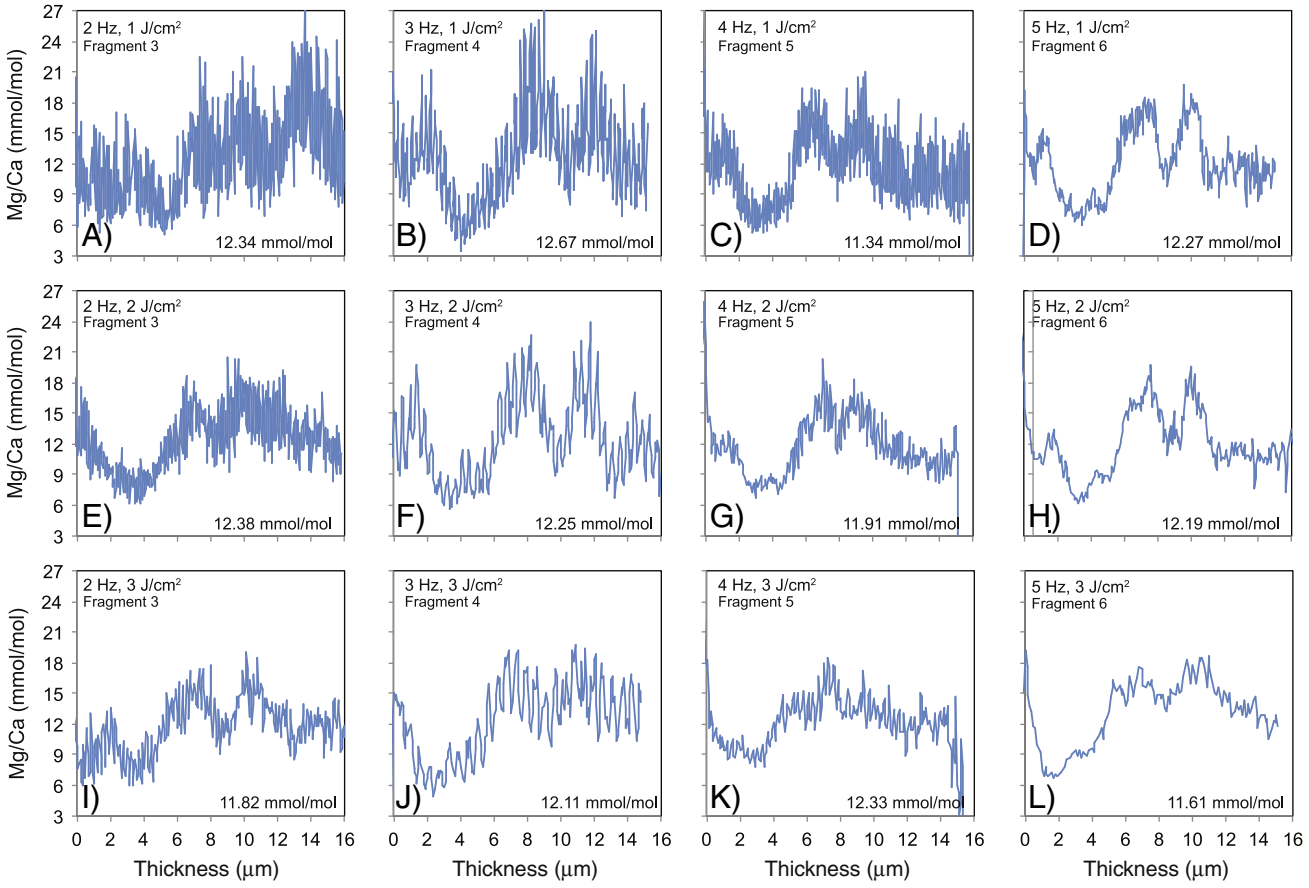

Fig. 3. Matrix of LA-ICP-MS results (without a squid) for a single *O. universa* using different energies and laser repetition rates. Shell was ablated from the interior surface to the exterior surface. MS sweep time: ~300 ms. Average Mg/Ca ratio is noted in the lower right corner of each plot.

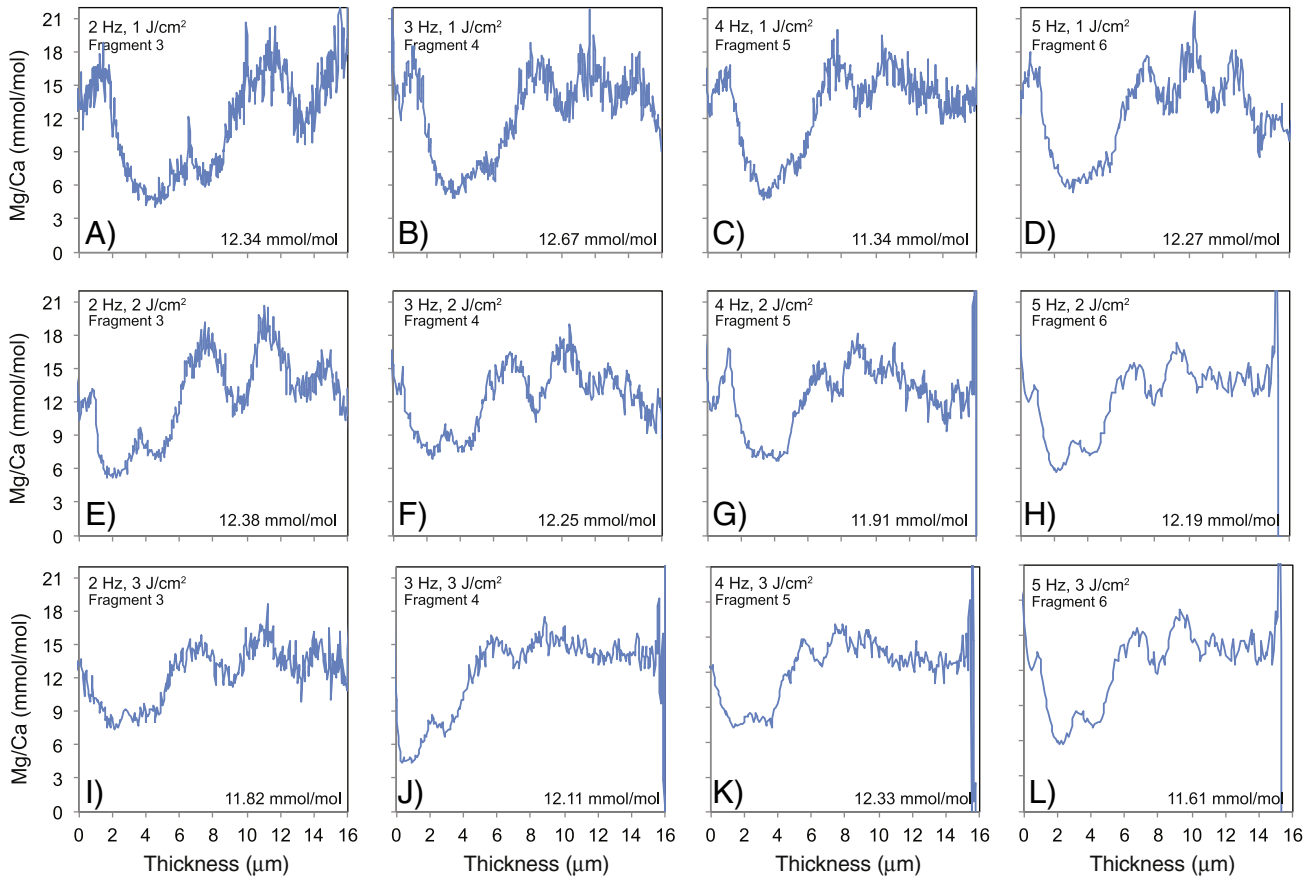

Fig. 4. Matrix of LA-ICP-MS results (with a squid) for a single *O. universa* using different energies and laser repetition rates. Shell was ablated from the interior surface to the exterior surface. MS sweep time: ~300 ms. Average Mg/Ca ratio is noted in the lower right corner of each plot.

laser pulse ablates more material than at lower energies, thereby averaging more of the fine-scale variability within the shell wall (e.g. Fig. 3L).

3.2.2. Depth profiles generated with a squid

The use of a squid within the sample gas flow path dampens the transient signal produced by the laser harmonics (Fig. 4). With the squid installed, high frequency Mg/Ca oscillations still occur as an artifact at various combinations of low energies (1–2 J/cm^2) and low repetition rates (2–4 Hz), but the amplitude (<5 mmol/mol) is lower than in the profiles produced without the squid. These oscillations are most pronounced when the laser energy is low (1 J/cm^2) and the repetition rate is ≤4 Hz (Fig. 4A–C). At intermediate repetition rates (3–5 Hz) and a moderate energy density (2–3 J/cm^2), such oscillations are virtually absent when the squid is installed (Fig. 4F–H, and J). Note that the decrease in the signal noise at higher repetition rates is not solely due to improved counting statistics (e.g. more material supplied to the mass spectrometer at higher repetition rates). As detailed in the supplement, increasing the counting statistics by using a larger spot size (additional ablated material/pulse) does not eliminate the beating effects that occur at lower repetition rates (Figures S10 and S11). Similar to results collected without the squid, we observed a decrease in spatial depth resolution when the laser energy density is 3 J/cm^2 (e.g., Fig. 4K and L).

The experiment described above utilizes *O. universa* shells, which are known to contain bands of high and low Mg/Ca ratios that can differ by >8 mmol/mol (Eggins et al., 2003). By optimizing laser ablation and ICP-MS settings, we are able to resolve more subtle intrashell Mg/Ca variation in shells where the amplitude of the Mg/Ca banding is lower (e.g. 3 mmol/mol). For example, *N. dutertrei* shells can contain alternating bands of high and low Mg/Ca calcite that are of lower amplitude than other planktic species (Fehrenbacher and Martin, 2010). Using a 5 Hz repetition rate, a moderate energy density (1.5 J/cm^2), and a ~300 ms cycle time, we are able to resolve these lower amplitude Mg/Ca variations in a specimen of *N. dutertrei* (Fig. 5). The optimized laser ablation settings were necessary to resolve these intrashell Mg/Ca variations.

Based on the results detailed in Figs. 3 and 4, we find that the operating parameters that produce the highest spatially resolved depth profiles with minimal harmonic oscillations is an ablation rate between 3–5 Hz and energy density greater than 1, but less than 3 J/cm^2 when the ICP-MS cycle time is ~300 ms. These optimized settings are a function of the cycle time we used for our particular analyses (Table 2, Method 5). A different ICP-MS cycle time with different analytes would likely require a different optimized repetition rate and/or energy density in order to minimize interferences between the repetition rate and MS cycle time. Note that we have also been able to produce high-resolution profiles using a longer cycle time with these same laser settings (Vetter et al., 2013b). Reasonable depth profiles can be generated without using a squid when using higher repetition rates (5 Hz) and moderate laser energies (>1, but <3 J/cm^2) (e.g. Fig. 3H), however, using the squid minimizes harmonic oscillations of varying amplitude in the Mg/Ca ratios (e.g. compare Figs. 3G and 4G; 3H and 4H). Our results show that one should avoid using repetition rates and cycle times that have a similar temporal beat (e.g. a 250 ms cycle time with a 4 Hz repetition rate) in order to avoid harmonic artifacts. This issue is particularly problematic if dwell times are similar for all masses.

3.3. Foraminifera 'reference material' and inter-laboratory comparisons

In order to generate reproducible high-resolution depth profiles and compare data and instrument performance within and between

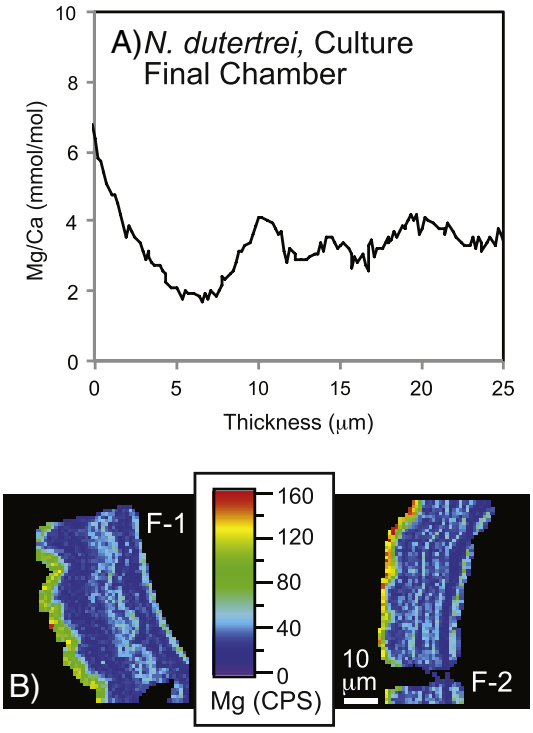

Fig. 5. A. Mg/Ca laser ablation profile (ablated from the outer to inner surface) of the F-3 chamber of an *N. dutertrei* shell collected by plankton net and maintained in the laboratory. B. An electron microprobe image map of Mg counts generated on the F-1 and F-2 chamber of the same specimen. Note that the Mg bands within the shell wall are resolvable using both analytical techniques (EMPA and LA-ICP-MS). The elevated Mg/Ca on the outer surface of the shell is from calcite precipitated in the laboratory at 18 °C. We estimate the pre-culture temperature in which the specimen grew was ~10 °C. This specimen completed its lifecycle and underwent gametogenesis in the laboratory.

analytical sessions it is desirable to use a reference material that is matrix-matched with foraminifera and yields measurable elemental variation that is reproducible. At UC Davis, we use randomly selected fossil *O. universa* shells for this purpose. *O. universa* fragments from the same shell can be used as a reference material for assessing reproducibility within and between analytical sessions especially when analyzing specimens for which replicate ablations are not possible (e.g. very small foraminifers such as *Neogloboquadrina pachyderma*) (Figure S1). A second potential use for *O. universa* fragments could be in cross calibration studies between laboratories, where material from different shells could be distributed and used to bridge interlaboratory standardization for depth profile analyses. To our knowledge, no other species of foraminifera or matrix-matched material is widely available for such an application. Our within-fragment Mg/Ca precision (2σ), based on 6 fragments analyzed between 2 and 5 times each over a 5 month period, ranged from 0.1–0.6 mmol/mol, or 1–7% of the mean shell ratio. Repeat profiles from closely spaced regions in a shell have the most similar Mg/Ca profiles, but all profiles from the same shell display the same distinct minima and maxima ratios and patterns (Figure S1). Reproducibility (2σ) of the mean whole-shell Mg/Ca ratio, based on all measurements (multiple profiles on all fragments; N = 30), is ~0.8 mmol/mol Mg/Ca (~8%).

4. Concluding remarks

In this study, we illustrate how the quality, clarity, and spatial resolution of laser ablation depth profiles can be markedly improved by modifying the repetition rate of the laser, the total cycle time of the ICP-MS, and/or by using a squid. For assessing intrashell Mg/Ca variation, we find that a combination of a moderate repetition rate (4–5 Hz), low energy density between 1 and 3 J/cm^2, and use of a squid produces high-resolution laser ablation profiles with little to no spectral skew. High-amplitude, high-frequency oscillations in Mg/Ca profiles are generated when the laser repetition rate is similar to or less than the cycle time of the mass spectrometer, regardless of whether or not a squid is used. However, the use of a squid reduces the amplitude of these oscillations. Careful optimization of analytical conditions using the approach presented here can improve the resolution of depth profiles and produce spatially resolved data that reflect real TE/Ca variability. Our results confirm that if only average whole-shell TE/Ca ratios are desired and intrashell variation is not needed, then a range of repetition rates and energy densities can be used to produce accurate average ratios. However, important intrashell variability could go undetected if LA-ICP-MS optimization is not established before generating elemental depth profiles in foraminiferal shells.

Acknowledgments

We thank S. Shuttleworth and J. Roy (Photon Machines) and J. Wimpenny (LLNL) for valuable suggestions and instructive feedback during the installation, optimization, and calibration of the laser ablation facility. We also acknowledge NSF awards 0550703, 0946297 and 1061676 (HJS) and 1261519 (JSF and ADR) for research support. We also thank three anonymous reviewers whose comments greatly improved an earlier version of this manuscript.

Appendix A. Supplementary data

Supplementary data to this article can be found online at http://dx.doi.org/10.1016/j.chemgeo.2015.04.007.

References

Allen, K.A., Hoenisch, B., Eggins, S.M., Rosenthal, Y., 2012. Environmental controls on B/Ca in calcite tests of the tropical planktic foraminifer species *Globigerinoides ruber* and *Globigerinoides sacculifer*. Earth Planet. Sci. Lett. 351, 270–280.
Anand, P., Elderfield, H., Conte, M.H., 2003. Calibration of Mg/Ca thermometry in planktonic foraminifera from a sediment trap time series. Paleoceanography 18 (2), 15.
Barker, S., Elderfield, H., 2002. Foraminiferal calcification response to glacial–interglacial changes in atmospheric CO_2. Science 297 (5582), 833–836.
Bolton, A., Baker, J.A., Dunbar, G.B., Carter, L., Smith, E.G.C., Neil, H.L., 2011. Environmental versus biological controls on Mg/Ca variability in *Globigerinoides ruber* (white) from core top and plankton tow samples in the southwest Pacific Ocean. Paleoceanography 26.
Boyle, E.A., 1988. Cadmium: chemical tracer of deep-water paleoceanography. Paleoceanography 3 (471e490), 48.
Creech, J.B., Baker, J.A., Hollis, C.J., Morgans, H.E.G., Smith, E.G.C., 2010. Eocene sea temperatures for the mid-latitude southwest Pacific from Mg/Ca ratios in planktonic and benthic foraminifera. Earth Planet. Sci. Lett. 299 (3–4), 483–495.
de Garidel-Thoron, T., Rosenthal, Y., Beaufort, L., Bard, E., Sonzogni, C., Mix, A.C., 2007. A multiproxy assessment of the western equatorial Pacific hydrography during the last 30 kyr. Paleoceanography 22.
de Villiers, S., 2003. Dissolution effects on foraminiferal Mg/Ca records of sea surface temperature in the western equatorial Pacific. Paleoceanography 18 (3).
Duenas-Bohorquez, A., da Rocha, R.E., Kuroyanagi, A., Bijma, J., Reichart, G.-J., 2009. Effect of salinity and seawater calcite saturation state on Mg and Sr incorporation in cultured planktonic foraminifera. Mar. Micropaleontol. 73 (3–4), 520–522.
Eggins, S.M., Kinsley, L.K., Shelley JMG, J.M.G., 1998a. Deposition and element fractionation processes occurring during atmospheric pressure laser sampling for analysis by ICPMS. Appl. Surf. Sci. 127–129, 278–286.
Eggins, S.M., Rudnick, R.L., McDonough, W.F., 1998b. The composition of peridotites and their minerals, a laser-ablation ICPMS study. Earth Planet. Sci. Lett. 154, 53–71.
Eggins, S., Deckker, P.D., Marshall, J., 2003. Mg/Ca variation in planktonic foraminifera tests: implications for reconstructing palaeo-seawater temperature and habitat migration. Earth Planet. Sci. Lett. 212, 291–306.
Eggins, S., Sadekov, A., Deckker, P.D., 2004. Modulation and daily banding of Mg/Ca in *Orbulina universa* tests by symbiont photosynthesis and respiration: a complication for seawater thermometry? Earth Planet. Sci. Lett. 225, 411–419.
Fehrenbacher, J., Martin, P., 2010. Mg/Ca variability of the planktonic foraminifera *G. ruber* s.s. and *N. dutertrei* from shallow and deep cores determined by electron microprobe image mapping. *IOP Conf. Ser.: Earth Environ. Science*, 9(012018).
Fehrenbacher, J., Martin, P., 2011. Western equatorial Pacific deep water carbonate chemistry during the Last Glacial Maximum and Deglaciation: using foraminiferal Mg/Ca to reconstruct temperature and dissolution. Paleoceanography 26.

Fehrenbacher, J., Martin, P.A., Eshel, G., 2006. Glacial deep water carbonate chemistry inferred from foraminiferal Mg/Ca: a case study from the western tropical Atlantic. Geochem. Geophys. Geosyst. 7.
Fehrenbacher, J.F., Spero, H.J., Russell, A.D., 2011. Observations of living non-spinose planktic foraminifers *Neogloboquadrina dutertrei* and *N. pachyderma* from specimens grown in culture. *American Geophysical Union, Fall Meeting 2011* (abstract #PP41A-1724).
Gunther, D., Hattendorf, B., 2005. Solid sample analysis using laser ablation inductively coupled plasma mass spectrometry. Trends Anal. Chem. 24 (3), 255–265.
Hathorne, E.C., Alard, O., James, R.H., Rogers, N.W., 2003. Determination of intratest variability of trace elements in foraminifera by laser ablation inductively coupled plasma-mass spectrometry. Geochem. Geophys. Geosyst. 4 (12).
Hathorne, E.C., James, R.H., Lampitt, R.S., 2009. Environmental versus biomineralization controls on the intratest variation in the trace element composition of the planktonic foraminifera *G. inflata* and *G. scitula*. Paleoceanography 24.
Jeffries, T., Jackson, S., Longerich, H., 1998. Application of a frequency quintupled Nd: YAG source ($\lambda = 213$ nm) for laser ablation inductively coupled plasma mass spectrometric analysis of minerals. J. Anal. At. Spectrom. 13 (9), 935–940.
Jochum, K.P., et al., 2011. Determination of reference values for NIST SRM 610–617 glasses following ISO Guidelines. Geostand. Geoanal. Res. 35 (4), 397–429.
Katz, M.E., Cramer, B.S., Franzese, A., Honisch, B., Miller, K.G., Rosenthal, Y., Wright, J.D., 2010. Traditional and emerging geochemical proxies in foraminifera. J. Foraminifer. Res. 40 (2), 165–192.
Lea, D.W., Mashiotta, T.A., Spero, H.J., 1999. Controls on magnesium and strontium uptake in planktonic foraminifera determined by live culturing. Geochim. Cosmochim. Acta 63 (16), 2369–2379.
Lea, D., Pak, D., Spero, H., 2000. Climate impact of Late Quaternary equatorial Pacific sea surface temperature variations. Science 289, 1719–1724.
Longerich, H.P., Jackson, S.J., Gunther, D., 1996. Laser ablation inductively coupled plasma mass spectrometric transient signal data acquisition and analyte concentration calculation. J. Anal. At. Spectrom. 11, 899–904.
Marchitto, T.M., Lynch-Stieglitz, J., Hemming, S.R., 2005. Deep Pacific $CaCO_3$ compensation and glacial–interglacial atmospheric $CO(_2)$. Earth Planet. Sci. Lett. 231 (3–4), 317–336.
Marr, J.P., Baker, J.A., Carter, L., Allan, A.S.R., Dunbar, G.B., Bostock, H.C., 2011. Ecological and temperature controls on Mg/Ca ratios of *Globigerina bulloides* from the southwest Pacific Ocean. Paleoceanography 26, PA2209.
Martin, P.A., Lea, D.W., Rosenthal, Y., Shackleton, N.J., Sarnthein, M., Papenfuss, T., 2002. Quaternary deep sea temperature histories derived from benthic foraminiferal Mg/Ca. Earth Planet. Sci. Lett. 198 (1–2), 193–209.
McConnell, M.C., Thunell, R.C., 2005. Calibration of the planktonic foraminiferal Mg/Ca paleothermometer: sediment trap results from the Guaymas Basin, Gulf of California. Paleoceanography 20 (9).
Müller, W., Shelley, M., Miller, P., Broude, S., 2009. Initial performance metrics of a new custom-designed ArF excimer LA-ICPMS system coupled to a two-volume laser-ablation cell. J. Anal. At. Spectrom. 24, 209–214.
Nurnberg, D., Groeneveld, J., 2006. Pleistocene variability of the Subtropical Convergence at East Tasman Plateau: evidence from planktonic foraminiferal Mg/Ca (ODP Site 1172A). Geochem. Geophys. Geosyst. 7, 18.
Nurnberg, D., Bijma, J., Hemleben, C., 1996. Assessing the reliability of magnesium in foraminiferal calcite as a proxy for water mass temperatures. Geochim. Cosmochim. Acta 60 (5), 803–814.
Pettke, T., Heinrich, C.A., Ciocan, A.C., Gunther, D., 2000. Quadrupole mass spectrometry and optical emission spectroscopy: detection capabilities and representative sampling of short transient signals from laser-ablation. J. Anal. At. Spectrom. 15 (9), 1149–1155.
Raitzsch, M., Duenas-Bohorquez, A., Reichart, G.J., de Nooijer, L.J., Bickert, T., 2010. Incorporation of Mg and Sr in calcite of cultured benthic foraminifera: impact of calcium concentration and associated calcite saturation state. Biogeosciences 7 (3), 869–881.
Raitzsch, M., Hathorne, E.C., Kuhnert, H., Groeneveld, J., Bickert, T., 2011. Modern and late Pleistocene B/Ca ratios of the benthic foraminifer *Planulina wuellerstorfi* determined with laser ablation ICP-MS. Geology 39 (11), 1039–1042.
Regenberg, M., Nurnberg, D., Steph, S., Groeneveld, J., Garbe-Schonberg, D., Tiedemann, R., Dullo, W.C., 2006. Assessing the effect of dissolution on planktonic foraminiferal Mg/Ca ratios: evidence from Caribbean core tops. Geochem. Geophys. Geosyst. 7.
Rosenthal, Y., Lohmann, G.P., 2002. Accurate estimation of sea surface temperatures using dissolution-corrected calibrations for Mg/Ca paleothermometry. Paleoceanography 17 (3).
Rosenthal, Y., Field, M.P., Sherrell, R.M., 1999. Precise determination of element/calcium ratios in calcarious samples using sector field inductively coupled plasma mass spectrometry. Anal. Chem. 71 (15), 3248–3253.
Russell, A.D., Honisch, B., Spero, H.J., Lea, D.W., 2004. Effects of seawater carbonate ion concentration and temperature on shell U, Mg, and Sr in cultured planktonic foraminifera. Geochim. Cosmochim. Acta 68 (21), 4347–4361.
Sadekov, A., Eggins, S.M., De Deckker, P., Ninnemann, U., Kuhnt, W., Bassinot, F., 2009. Surface and subsurface seawater temperature reconstruction using Mg/Ca microanalysis of planktonic foraminifera *Globigerinoides ruber*, *Globigerinoides sacculifer*, and *Pulleniatina obliquiloculata*. Paleoceanography 24 (3).
Sadekov, A.Y., Eggins, S.M., Klinkhammer, G.P., Rosenthal, Y., 2010. Effects of seafloor and laboratory dissolution on the Mg/Ca composition of *Globigerinoides sacculifer* and *Orbulina universa* tests — a laser ablation ICPMS microanalysis perspective. Earth Planet. Sci. Lett. 292 (3–4), 312–324.
Shuxi, C., Shackleton, N.J., 1990. New technique for study on isotopic fractionation between sea water and foraminiferal growing processes. Chin. J. Oceanol. Limnol. 8 (4), 299–305.
Spero, H., Eggins, S.M., Russell, A.D., Vetter, L., Kilburn, M.R., Honisch, B., 2015. Timing and mechanism for intratest Mg/Ca variability in a living planktic foraminifer. Earth Planet. Sci. Lett. 409, 32–42.
Vetter, L., Kozdon, R., Mora, C., Eggins, S., Valley, J.W., Honisch, B., Spero, H.J., 2013a. Micron-scale intrashell oxygen isotope variation in cultured foraminifers. Geochim. Cosmochim. Acta 107, 267–278.
Vetter, L., Spero, H.J., Russell, A.D., Fehrenbacher, J.F., 2013b. LA-ICP-MS depth profiling perspective on cleaning protocols for elemental analysis in planktic foraminifers. Geochem. Geophys. Geosyst. 14 (8).
von Langen, P.J., Pak, D., Spero, H., Lea, D., 2005. Effects of temperature on Mg/Ca in neogloboquadrinid shells determined by live culturing. Geochem. Geophys. Geosyst. 6 (Q10P03).
Wit, J.C., Reichart, G.J., Jung, S.J.A., Kroon, D., 2010. Approaches to unravel seasonality in sea surface temperatures using paired single-specimen foraminiferal delta(18)O and Mg/Ca analyses. Paleoceanography 25.
Wit, J.C., de Nooijer, L.J., Barras, C., Jorissen, F., Reichart, G.J., 2012. A reappraisal of the vital effect in benthic foraminifera on Mg/Ca ratios: species specific uncertainty relationships. Biogeosciences 9.
Wu, G., Hillaire-Marcel, C., 1995. Application of LP-ICP-MS to benthic foraminifers. Geochim. Cosmochim. Acta 59 (2), 409–414.
Yu, J.M., Elderfield, H., 2007. Benthic foraminiferal B/Ca ratios reflect deep water carbonate saturation state. Earth Planet. Sci. Lett. 258 (1–2), 73–86.

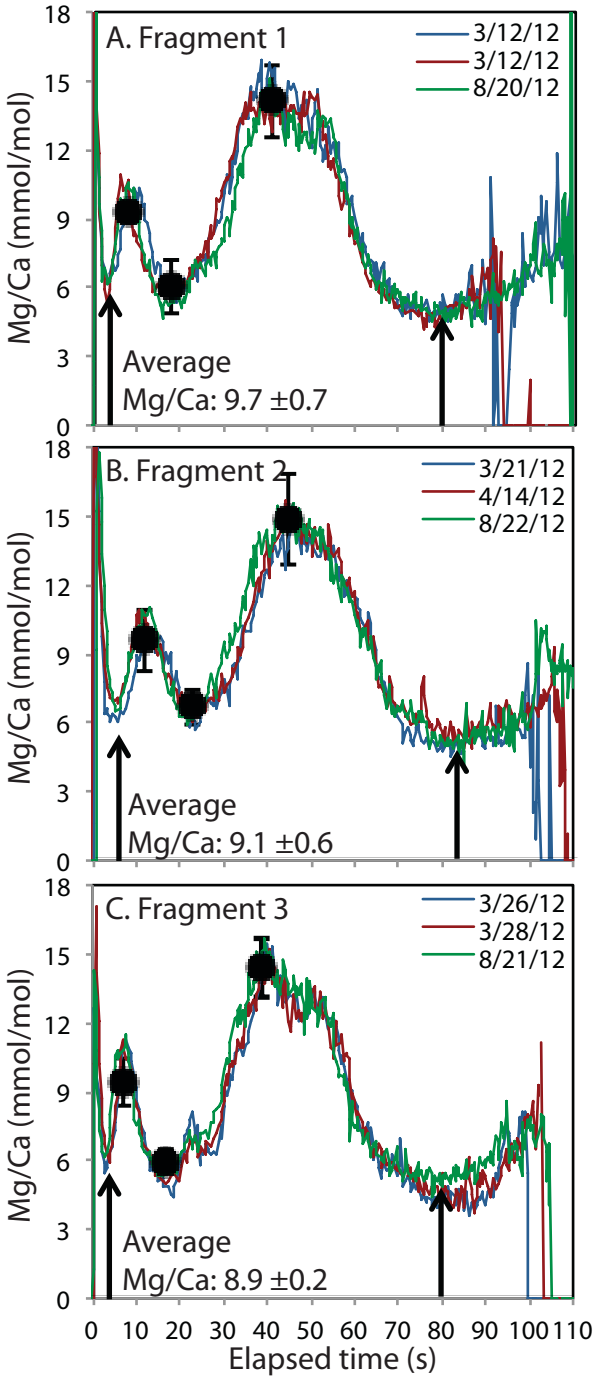

Figure S1:
Repeat profiles through 3 different fragments of an *O. universa* shell that we use to assess depth profile reproducibility (Sweep time: ~300ms, Repetition rate: 5 Hz, Fluence: 1.5 J/cm^2). Profiles through the same fragment (i.e. laser pits that are in closest proximity to one another) have the most similar Mg/Ca profiles. Average ratios are calculated by integrating all measurements between the black arrows, which mark the beginning of the shell analysis and an ending point that is similar for each profile. We attribute the increased variability at the end of the profiles to possible wall effects and decreased beam focusing as the depth of the laser ablation hole increases [*Eggins et al.,* 1998, *Eggins et al.,* 2003]. Note the ablation profiles do not end at the same time because of variability in the exact time that the laser breaks through the shell fragment. Circle symbols identify the average Mg/Ca ratio calculated at the Mg/Ca maxima and minima in the shell profiles as calculated by averaging 3 seconds of analyses time on each side of the maximum/minimum peak). The error bars denote 2σ standard deviation of the mean.

Figure S2: Washout time comparison when the squid is installed (A) vs. no squid (B). Complete washout occurs within 2 seconds without a squid. The washout time increases to ~3.5 seconds when the squid is installed. Note the delay from background to peak counts is also longer when the squid is installed.

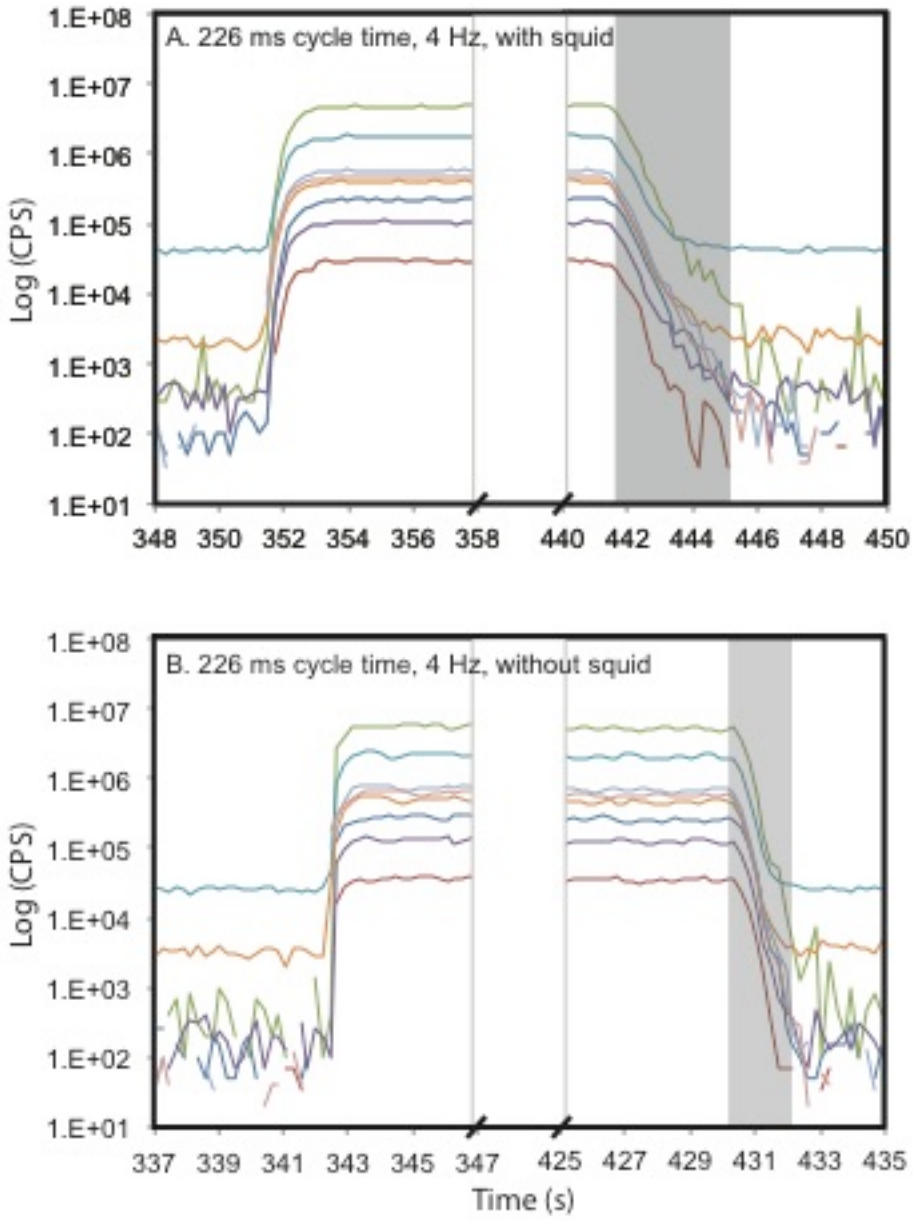

Figure S3: Example ablation profile through an *Orbulina universa* shell. Data integration begins after the initial spike in the counts stabilizes (potentially due to surface contamination). The rapid decrease in the Ca counts that is coincident with the rise in ^{27}Al is due to ablation of the carbon tape, and marks the end of data collection. Elemental ratios decrease abruptly when the laser is turned off.

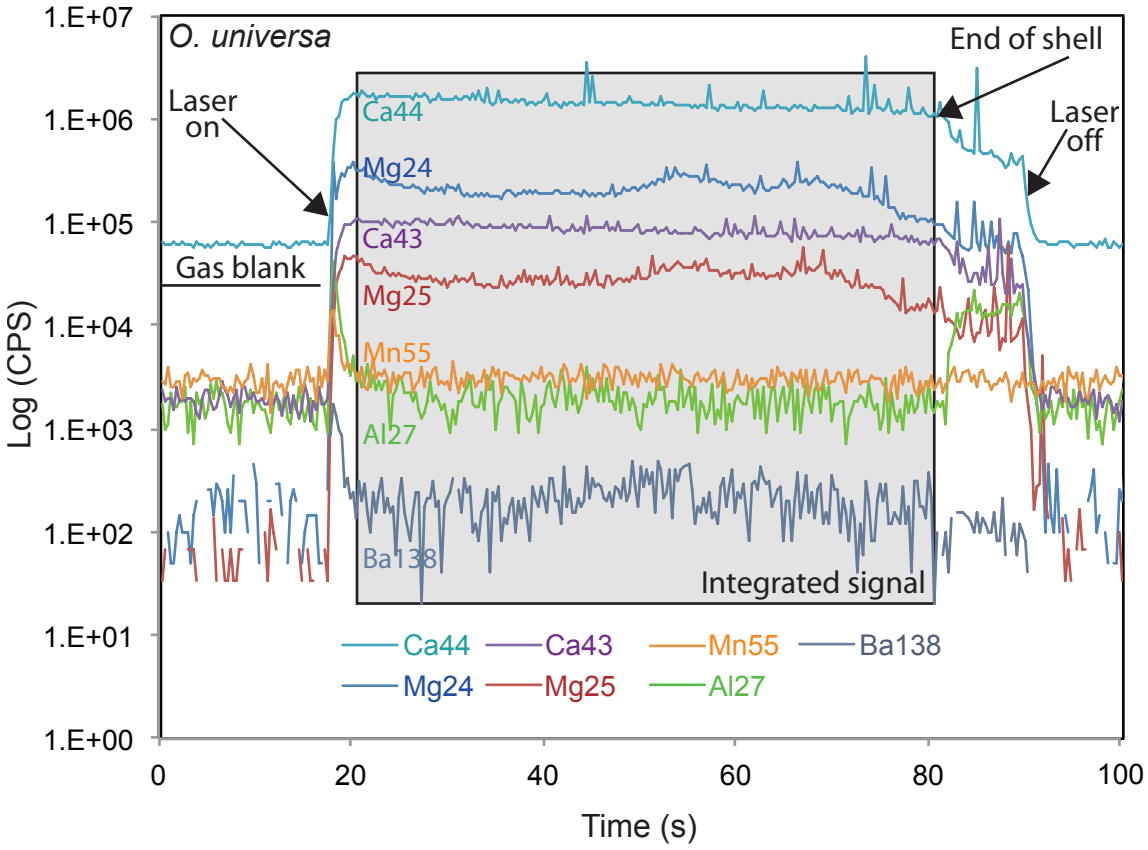

Figure S4: Laser ablation line scans on NIST 610 generated without (left panels) and with (right panels) a squid installed. Repetition rates range from 1 to 8 Hz and the mass spectrometer isotope menus as described in Table 2. See Figures S5 and S6 or more detail on Mg/Ca and Figures S7 and S8 for more detail on Sr/Ca.

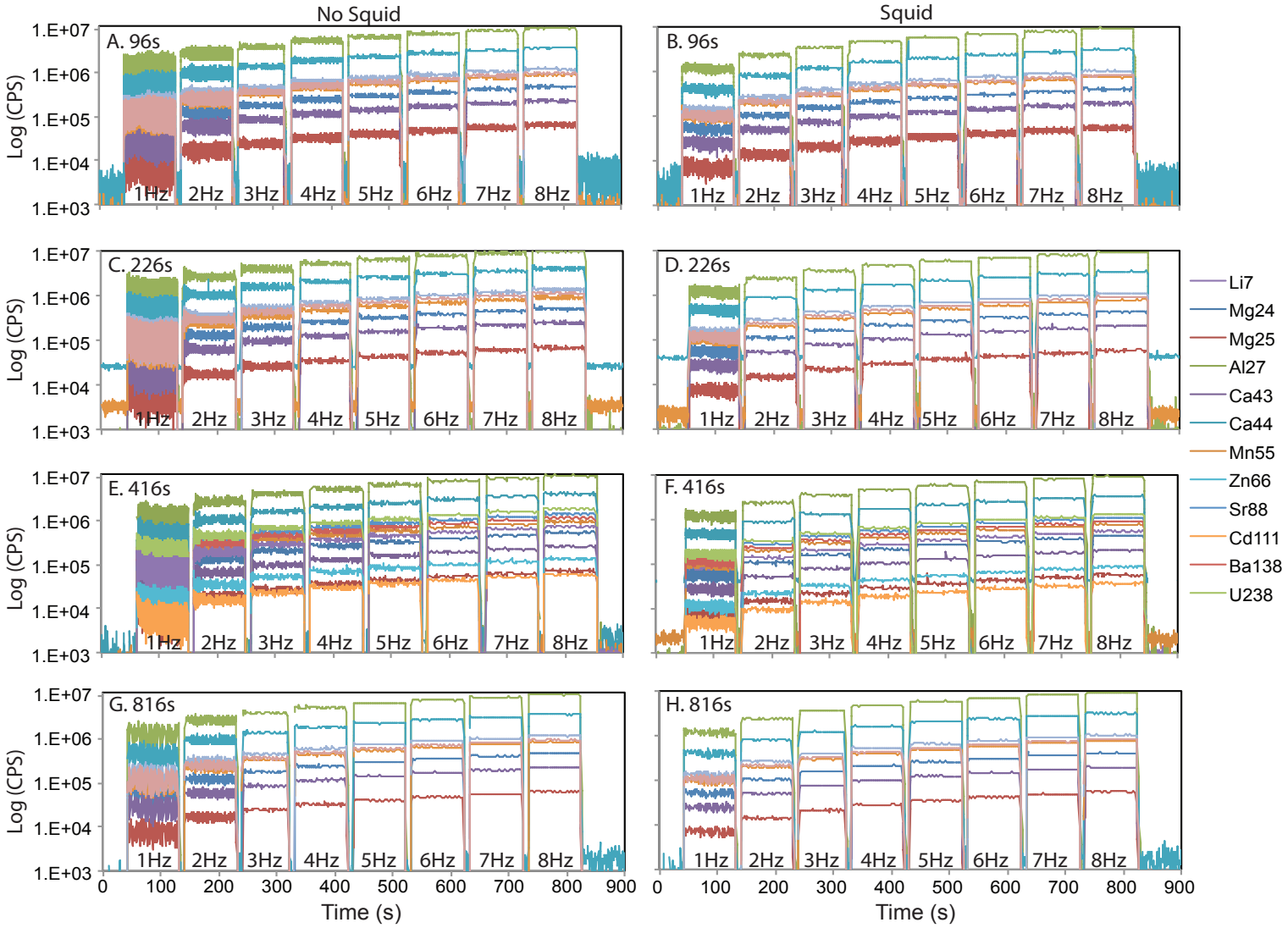

Figure S5: Expanded regions of Figure S4 Mg/Ca (cps/cps) for the 96 ms (A-F) and 226 ms (G-L) mass spectrometer cycle without the squid (A-C, G-I) and with the squid (D-F, J-L).

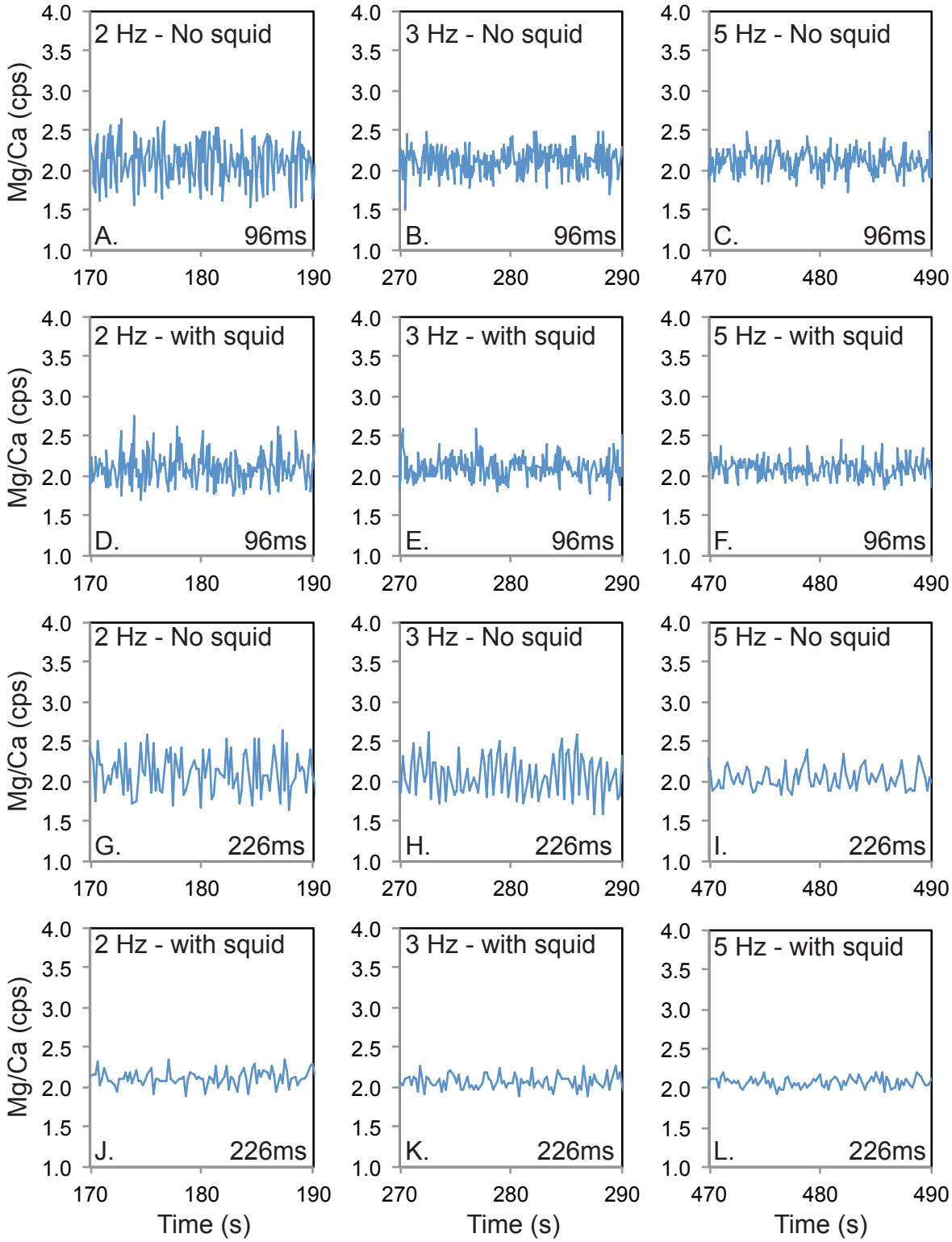

Figure S6: Expanded regions of Figure S4 Mg/Ca (cps/cps) for the 426 ms (A-F) and 816 ms (G-L) mass spectrometer cycle without the squid (A-C, G-I) and with the squid (D-F, J-L).

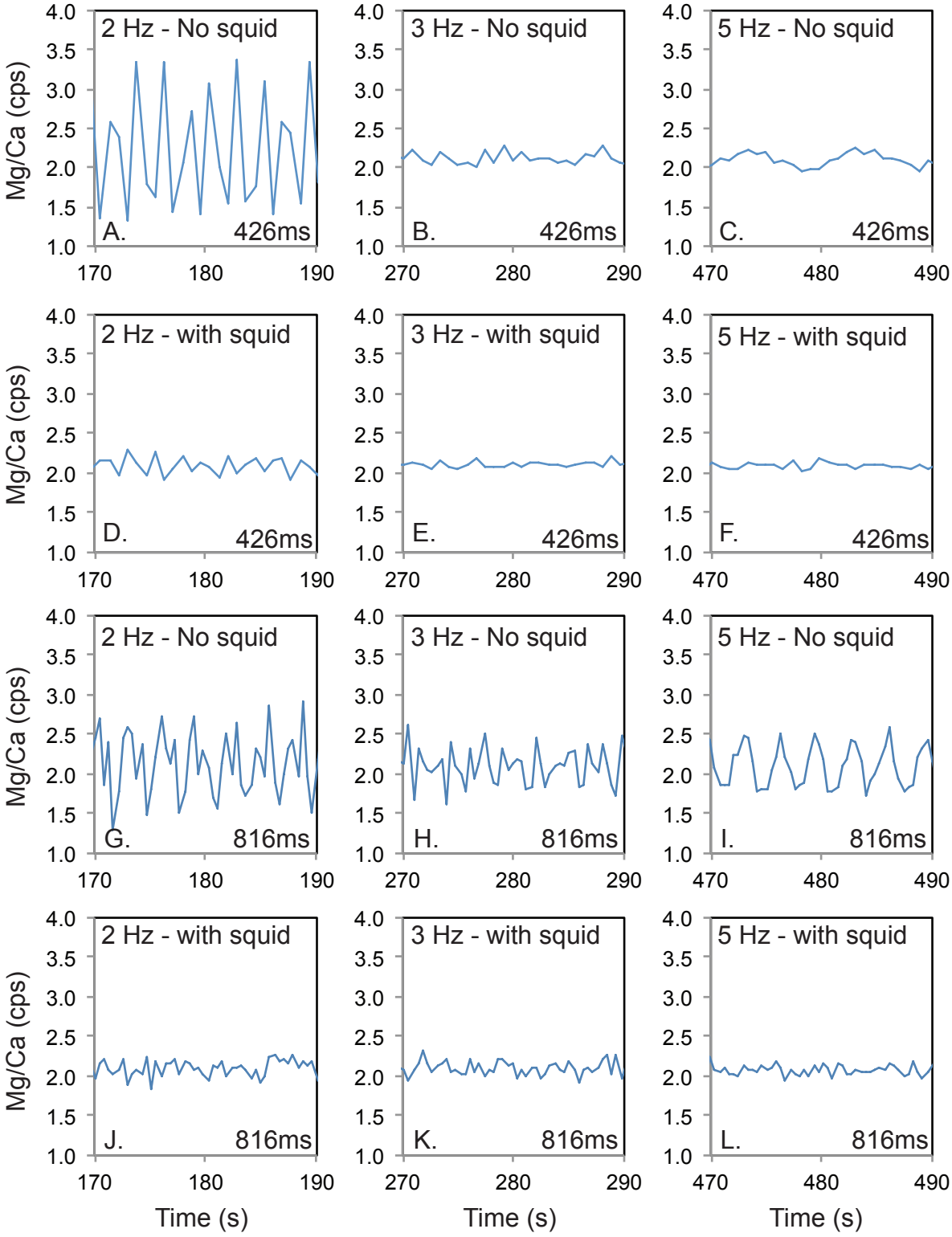

Figure S7: Expanded regions of Figure S4 Sr/Ca (cps/cps) for the 96 ms (A-F) and 226 ms (G-L) mass spectrometer cycle without the squid (A-C, G-I) and with the squid (D-F, J-L).

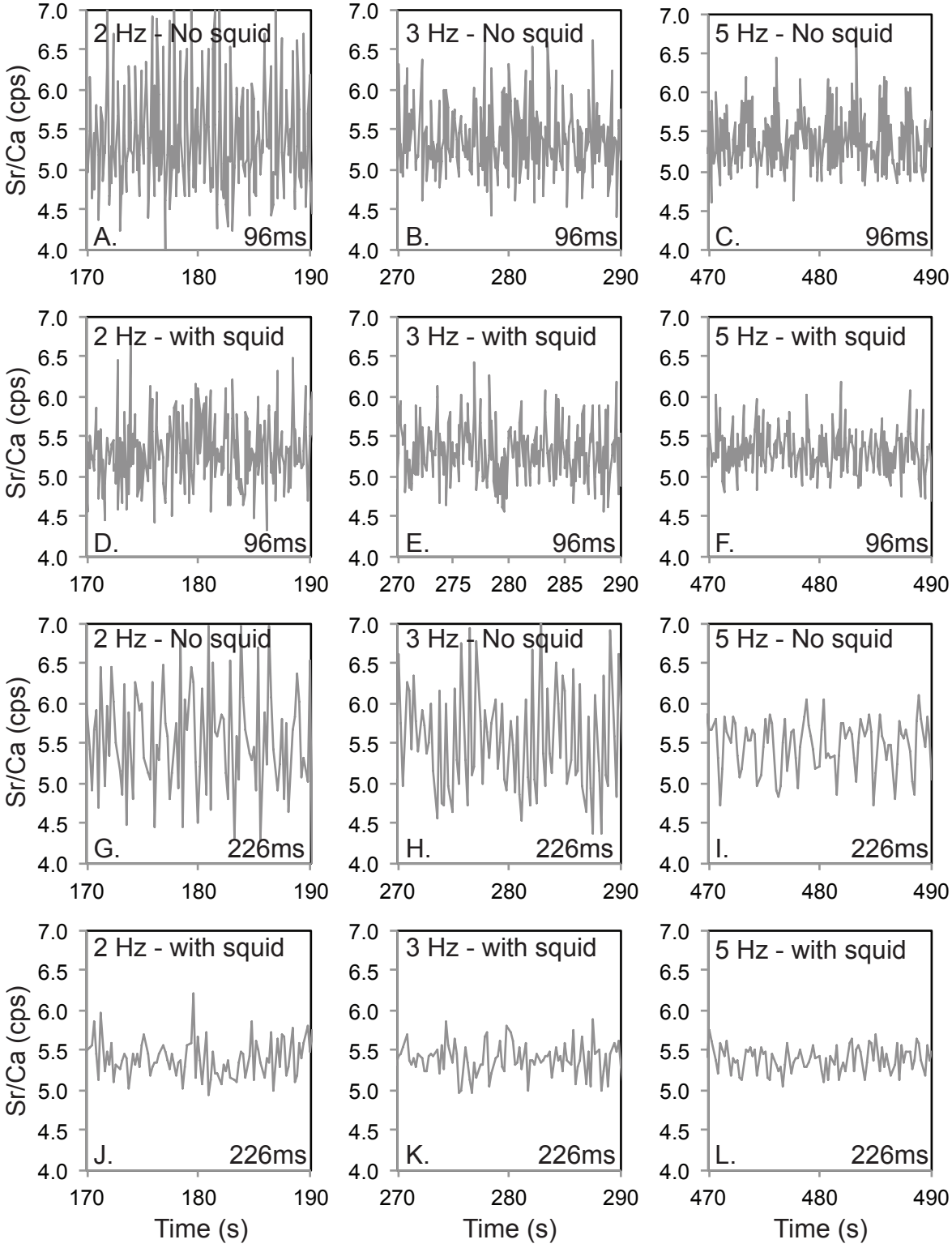

Figure S8: Expanded regions of Figure S4 Sr/Ca (cps/cps) for the 426 ms (A-F) and 816 ms (G-L) mass spectrometer cycle without the squid (A-C, G-I) and with the squid (D-F, J-L).

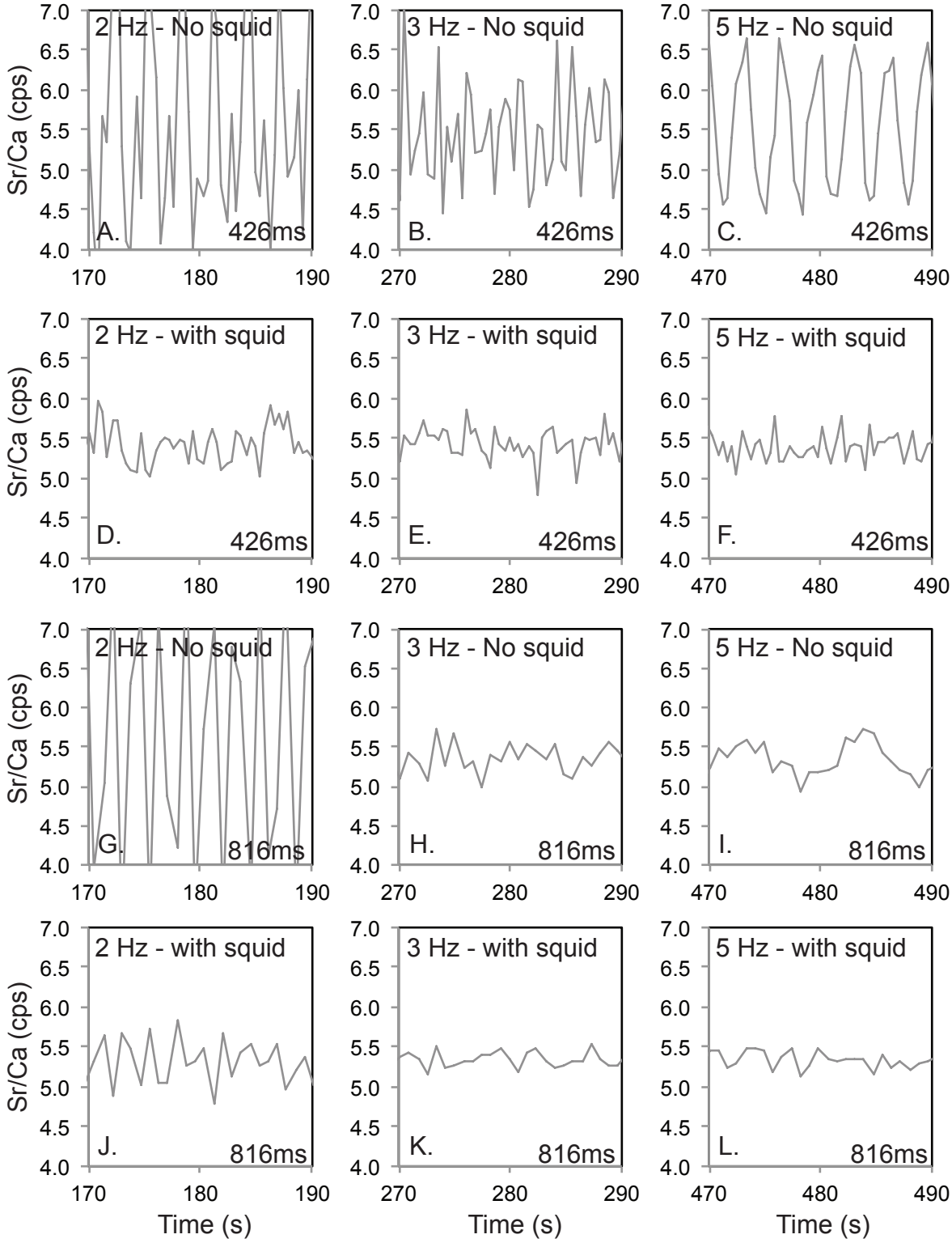

Figure S9:
This figure illustrates differences in the magnitude and timing of the high-amplitude oscillations that can occur when the repetition rate of the laser (one pulse every 333 ms) and the mass spectrometer cycle time (~300 ms) are similar. In this case, we used an energy density of 1.5 J/cm^2 and a repetition rate of 3 Hz (A and C) and 6 Hz (B and D) both with (A and B) and without (C and D) the squid. The figures generated without the squid also contain a 5-pt running mean of the data (heavy black line).

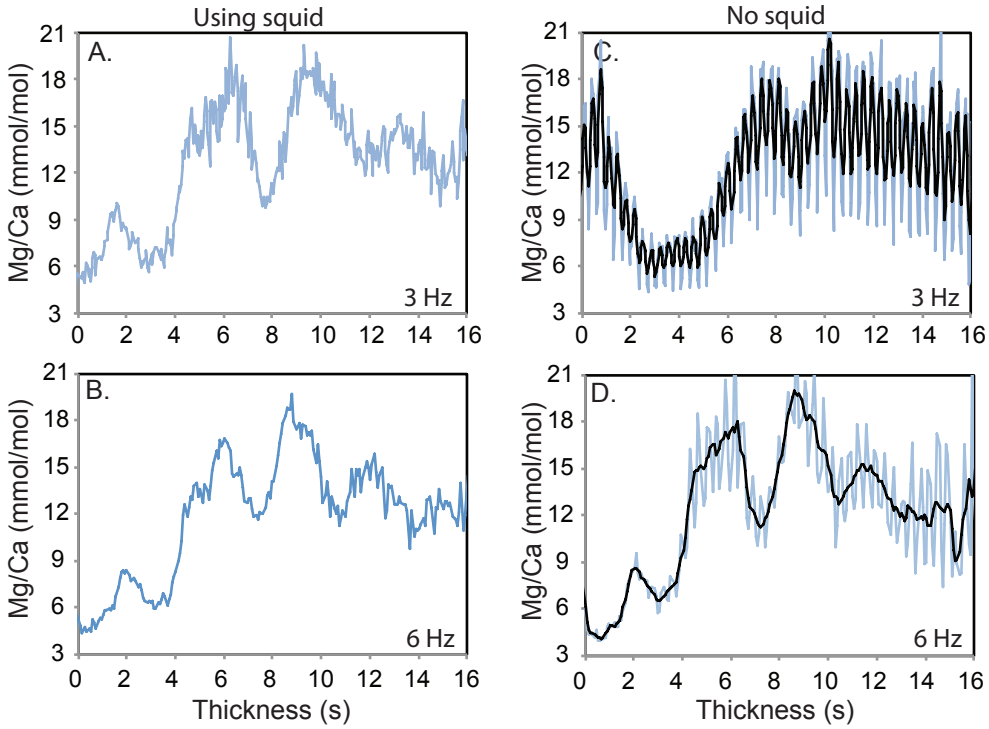

In an effort to disentangle the effects of counting statistics vs. repetition rate, additional depth profiles were generated at two energies (1.1 J/cm2 and 1.6 J/cm2), two repetition rates, (2 and 4 Hz) and two spot sizes (40 and 65 μm). The increase in spot size from 40 μm to 65 μm increases the ICPMS signal ~2.5 times. The results show that regardless of spot size, there is still a 'beating effect' when using the lower, 2 Hz, repetition rate. This 'beat effect' is more problematic when using lower energies (1.1 J/cm^2; Figure S10. Plot A) and if a foraminifer had transitions in shell chemistry that were very close together, the 2 Hz repetition rate would be more problematic for data interpretation.

Figure S10: Depth profiles generated using a laser energy of 1.1 J/cm^2. A. Comparison of results at 2 Hz (40 and 65 μm spot sizes). B. Comparison of results at 4 Hz (40 and 65 μm spot sizes). Plots C and D are the same data plotted in A and B. The data here are plotted in order to directly compare results using the same spot size, but different repetition rates. C. 40 μm spot size D. 65 μm.

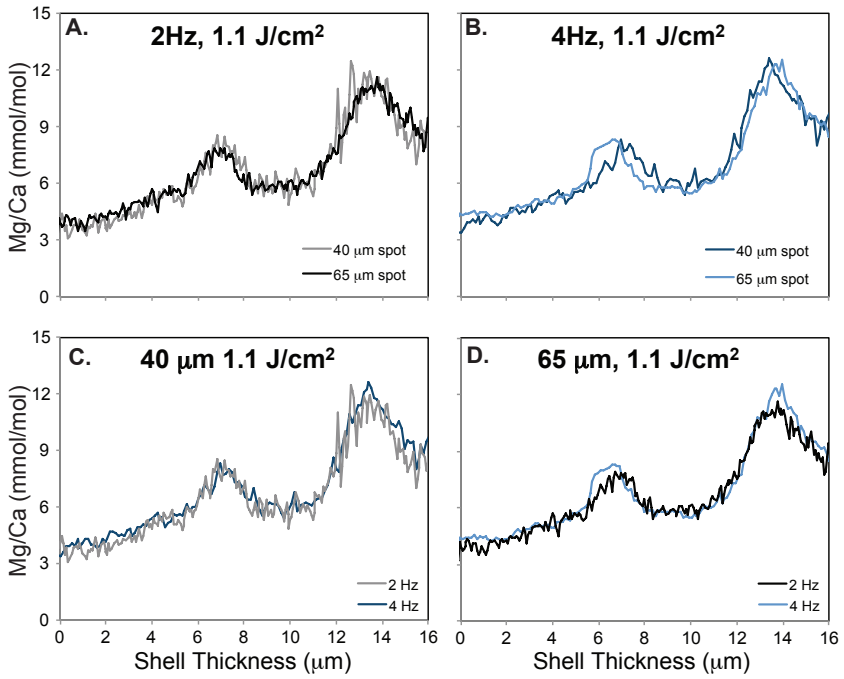

Figure S11: Depth profiles generated using a laser energy of 1.6 J/cm^2. A. Comparison of results at 2 Hz (40 and 65 μm spot sizes). B. Comparison of results at 4 Hz (40 and 65 μm spot sizes). Plots C and D are the same data plotted in A and B. The data here are plotted in order to directly compare results using the same spot size, but different repetition rates. C. 40 μm spot size D. 65 μm.

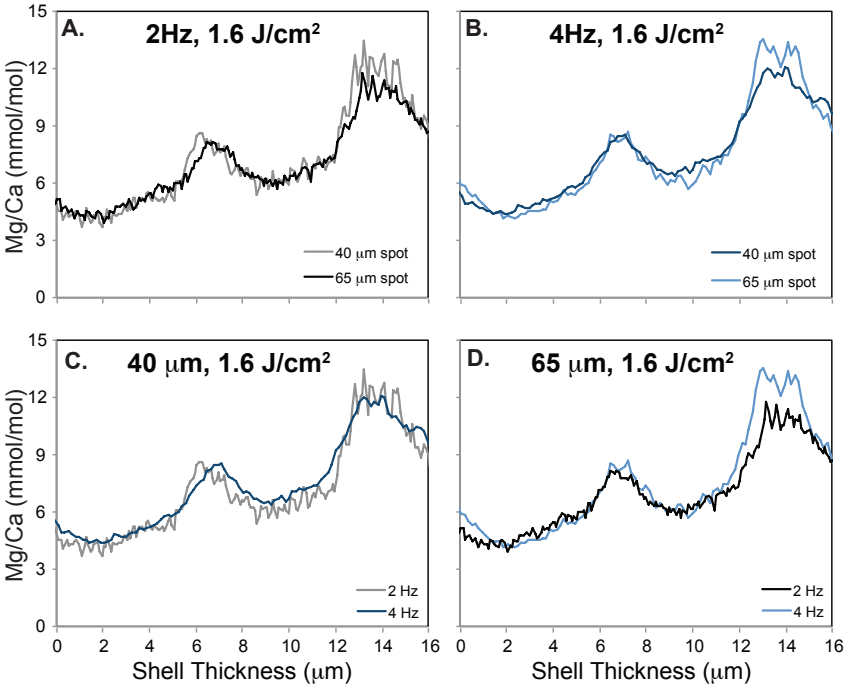

Table S1: Residual standard deviations for each cycle time/repetition rate combination

96 ms cycle time, With squid								
Hz	**Mg24**	**Mg25**	**Al27**	**Ca43**	**Ca44**	**Mn55**	**Sr88**	**Ba138**
1	14.1	20.9	13.3	15.7	12.4	13.7	14.0	14.0
2	6.1	12.1	4.9	7.8	5.0	5.6	5.5	5.6
3	4.9	9.9	3.8	6.2	3.9	4.1	4.4	4.3
4	4.8	8.9	4.0	6.0	4.1	4.2	4.2	4.4
5	3.9	7.6	3.1	5.0	5.6	3.4	3.3	3.4
6	3.8	7.1	3.1	4.9	3.2	3.3	3.4	3.3
7	3.0	6.2	2.1	3.9	2.2	2.5	2.4	2.7
8	3.3	6.1	2.6	4.0	2.6	2.7	2.8	2.9
96 ms cycle time, No squid								
Hz	**Mg24**	**Mg25**	**Al27**	**Ca43**	**Ca44**	**Mn55**	**Sr88**	**Ba138**
1	47.3	49.6	46.9	48.3	47.9	47.0	47.6	47.9
2	20.5	22.8	20.0	21.4	21.0	19.8	20.2	20.4
3	6.9	10.3	6.4	8.1	6.6	6.3	6.7	7.0
4	6.9	9.6	6.4	7.7	6.7	6.5	6.8	6.9
5	5.0	8.0	4.5	5.8	4.6	4.6	4.8	4.8
6	4.4	7.0	3.8	5.0	3.9	4.0	4.1	4.0
7	3.8	6.5	3.3	4.3	3.1	3.5	3.3	3.3
8	2.9	5.6	2.4	3.7	2.5	2.5	2.7	2.6

226 ms cycle time, With squid								
Hz	**Mg24**	**Mg25**	**Al27**	**Ca43**	**Ca44**	**Mn55**	**Sr88**	**Ba138**
1	18.6	19.1	17.8	17.9	18.0	17.9	17.8	17.5
2	4.0	7.0	3.8	4.1	3.2	3.6	3.4	2.9
3	3.4	5.4	3.3	3.6	3.1	3.2	2.8	2.3
4	3.0	4.5	2.6	3.2	2.3	2.5	2.2	1.8
5	2.6	4.7	2.5	2.8	2.0	2.3	1.9	1.8
6	2.3	3.8	2.3	2.7	2.1	2.1	1.9	1.7
7	2.4	3.9	2.1	2.8	1.9	2.0	1.8	1.6
8	2.1	3.5	2.0	2.2	1.8	1.9	1.7	1.5
226 ms cycle time, No squid								
Hz	**Mg24**	**Mg25**	**Al27**	**Ca43**	**Ca44**	**Mn55**	**Sr88**	**Ba138**
1	53.4	54.1	53.5	54.2	51.5	53.2	53.9	54.0
2	14.8	16.1	14.5	15.1	15.4	14.9	14.1	13.7
3	10.0	10.9	10.0	9.7	9.7	9.6	9.8	9.1
4	6.0	6.9	6.1	6.3	6.3	6.3	6.2	5.9
5	4.6	5.6	4.7	4.8	4.5	4.5	4.3	3.9
6	4.2	5.0	4.2	4.4	4.3	4.1	4.0	3.6
7	4.1	4.8	4.2	4.2	4.0	4.0	4.2	3.6
8	4.8	5.1	4.6	4.8	4.7	4.7	5.1	3.8

416 ms cycle time, With squid												
Hz	**Mg24**	**Mg25**	**Al27**	**Ca43**	**Ca44**	**Mn55**	**Sr88**	**Ba138**	**U238**	**Li7**	**Zn66**	**Cd111**
1	17.8	18.7	17.7	18.2	16.3	17.7	17.4	17.3	17.4	17.3	18.9	20.8
2	4.1	6.8	3.4	4.3	2.9	3.4	3.1	2.5	2.5	2.9	5.7	6.2
3	3.2	5.7	3.2	3.7	2.5	3.4	2.6	2.2	2.2	2.4	4.3	5.3
4	3.1	4.8	2.8	3.2	2.3	2.6	2.3	1.8	1.7	2.3	3.7	5.1
5	2.5	6.2	2.5	4.1	2.1	2.2	2.0	1.8	1.6	1.8	3.5	3.7
6	2.7	4.6	2.1	2.6	2.1	2.2	2.1	1.9	1.7	1.7	3.4	4.1
7	2.2	4.1	2.0	2.3	1.9	1.9	1.9	1.7	1.6	1.5	3.3	3.5
8	2.0	3.7	2.1	2.4	1.7	2.1	1.7	1.6	1.4	1.7	3.2	3.7
416 ms cycle time, No squid												
Hz	**Mg24**	**Mg25**	**Al27**	**Ca43**	**Ca44**	**Mn55**	**Sr88**	**Ba138**	**U238**	**Li7**	**Zn66**	**Cd111**
1	50.2	51.0	49.2	49.3	47.1	49.7	49.6	50.1	50.0	49.0	52.2	51.2
2	16.5	17.2	16.1	16.7	16.2	15.5	15.9	15.6	15.3	16.3	16.7	16.4
3	8.0	8.8	7.7	7.9	7.6	7.6	7.7	7.1	6.6	7.5	7.8	8.3
4	6.6	7.7	7.2	7.4	7.1	7.1	7.1	6.5	6.4	6.3	7.5	6.7
5	6.1	6.4	6.2	6.6	6.5	6.2	6.1	5.5	5.4	5.6	6.8	5.9
6	3.4	4.2	3.5	3.4	3.4	3.7	3.3	3.0	2.8	2.9	4.2	4.0
7	3.3	4.5	4.0	3.8	3.3	3.3	3.5	2.5	3.1	2.7	4.3	3.9
8	3.4	4.0	3.3	3.3	3.6	3.6	3.0	2.8	2.6	2.9	3.9	3.7

826 ms cycle time, With squid								
Hz	**Mg24**	**Mg25**	**Al27**	**Ca43**	**Ca44**	**Mn55**	**Sr88**	**Ba138**
1	12.9	14.8	12.7	13.5	13.0	13.1	13.2	13.3
2	3.0	4.3	2.9	3.9	2.9	2.9	3.3	3.5
3	1.7	3.0	1.4	1.8	1.6	1.5	1.6	1.6
4	2.0	2.9	1.7	2.1	1.8	2.0	2.0	1.9
5	1.5	2.5	1.3	1.7	1.4	1.4	1.2	1.4
6	1.2	2.4	1.1	1.5	1.2	1.2	1.1	1.2
7	1.9	2.2	1.0	1.5	1.0	1.0	1.0	1.0
8	1.1	1.8	1.0	1.5	1.0	1.2	1.0	1.0
826 ms cycle time, No squid								
Hz	**Mg24**	**Mg25**	**Al27**	**Ca43**	**Ca44**	**Mn55**	**Sr88**	**Ba138**
1	40.0	39.2	39.3	39.5	40.2	39.4	40.1	40.9
2	17.3	18.0	17.4	17.4	17.8	17.2	17.3	17.4
3	4.3	4.7	4.2	4.5	4.2	4.0	4.3	4.4
4	4.3	4.4	3.9	3.8	4.2	4.5	3.9	4.1
5	2.4	3.0	2.4	2.8	2.4	2.3	2.3	2.3
6	1.8	2.5	1.5	2.0	1.6	1.6	1.8	1.7
7	1.4	2.1	1.2	1.7	1.1	1.4	1.1	1.2
8	1.4	2.0	1.2	1.6	1.2	1.2	1.2	1.2